Eur. Phys. J. B **52**, 421–426 (2006)
DOI: 10.1140/epjb/e2006-00307-6

THE EUROPEAN PHYSICAL JOURNAL B

Multiple scattering investigation of the 1T-TaS_2 surface termination

L. Despont[1,a], F. Clerc[1], M.G. Garnier[1], H. Berger[2], L. Forró[2], and P. Aebi[1]

[1] Institut de Physique, Université de Neuchâtel, Rue A.-L. Breguet 1, 2000 Neuchâtel, Switzerland
[2] Institut de Physique de la Matière Complexe, EPFL, 1015 Lausanne, Switzerland

Received 3 April 2006 / Received in final form 3 July 2006
Published online 1st August 2006 –

Abstract. Multiple scattering theory based on a cluster model is used to simulate full hemispherical X-ray photoelectron diffraction measurements on a $1T$-TaS_2(0001) surface. Key points to determine the surface termination are discussed. As the commonly applied single scattering simulations do not give satisfying results, a multiple scattering approach has to be used to accurately simulate the full hemispherical photoelectron diffraction patterns. Differences and similarities between calculations of Ta and S terminated surfaces are presented along with experimental results at room temperature using both, the single and the multiple scattering approaches. We find that the surface is S terminated and that the quantitative difference between the calculations for both terminations permits to show the limits of the single scattering approach for solving surface termination problems. Moreover, by generalizing the results obtained using the multiple scattering approach, we discuss the application of this method to other similar systems.

PACS. 61.14.Qp X-ray photoelectron diffraction – 68.49.Jk Electron scattering from surfaces

Introduction

In general, the complete knowledge of the atom positions is necessary to understand the various properties of material's surfaces. Among the numerous techniques available to obtain information on the crystal structure, X-ray photoelectron diffraction (XPD) has proven to be very powerful, due to its chemical sensitivity and ability to measure sub-angstroem atomic displacements. However, without theoretical simulations it is often difficult to understand the different structures appearing in an XPD result and to rely them to true atomic positions. The use of multiple scattering (MSC) is unavoidable especially for bulk-emission XPD [1], as in the present case, because the simpler single scattering approach dramatically overemphasizes the so-called emitter-scatterer "forward focusing" effect, rendering the interpretation of finer interference features, which is necessary for the determination of the surface termination, very difficult.

Transition metal dichalcogenides are since long of strong interest because of their quasi-two-dimensional character, interesting electronic properties and various phase transitions. The basic structure of $1T$-TaS_2 is "sandwich-like": hexagonal planes of Ta are sandwiched by two hexagonal S planes leading to a quasi-two-dimensional material, see Figure 1. The forces between the sandwiches (of the magnitude of Van der Waals forces) are small, letting the layered crystal be easily cleaved (between two S layers as will be shown in the present article). Similar surfaces, i.e. MoS_2, $NbSe_2$ and $TiSe_2$, were studied in the past by dynamical low energy electron diffraction [2,3].

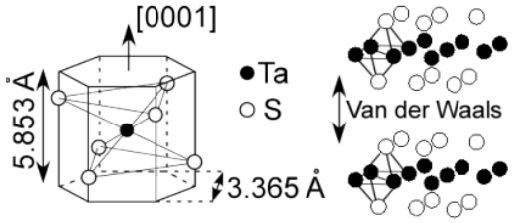

Fig. 1. Unit cell of $1T$-TaS_2. Ta atom (black) planes are "sandwiched" between the S atoms (white).

Here we investigate the $1T$-TaS_2 surface termination using room temperature XPD measurements together with MSC and SSC calculations. We show that the surface termination determination is very difficult using only the SSC approach while the MSC is more adapted to answer to this question. Furthermore we attempt to generalize this approach and discuss the applicability to other similar systems.

[a] e-mail: Laurent.Despont@Unine.ch

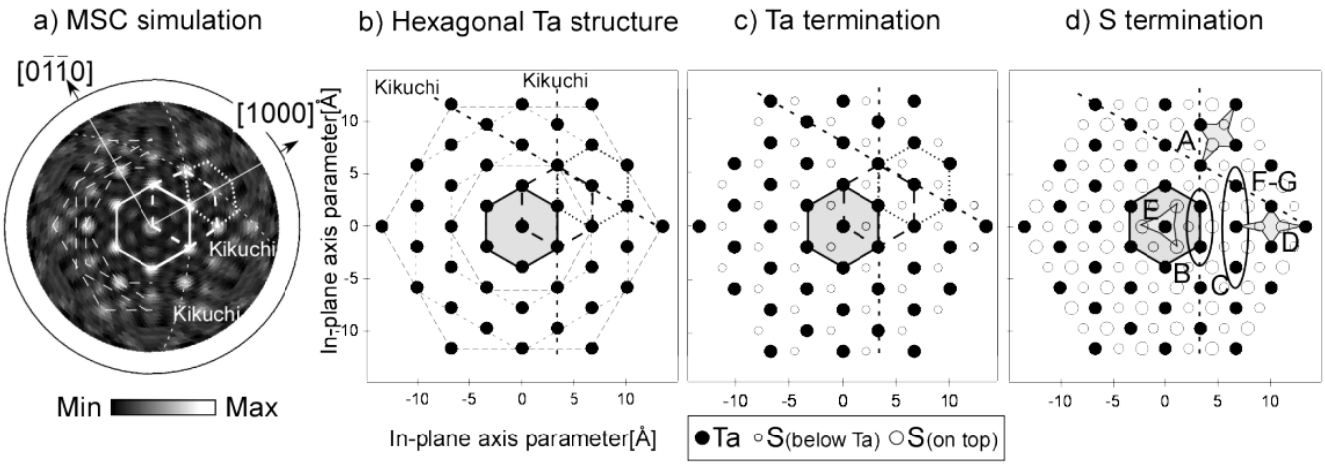

Fig. 2. (a) Stereographic projection of the calculated Ta $4f_{7/2}$ emission intensity of the structure shown in (b). In-plane cuts are displayed for (b) a hypothetical hexagonal Ta structure, (c) the Ta-terminated and (d) S-terminated surface. The two dashed lines in the (a)–(d) parts correspond to the low-index atomic planes from which the Kikuchi bands contained in the diffractograms originate. The labeled regions in the S-terminated cut are discussed in the text.

Experimental and computational details

Pure $1T$-TaS_2, prepared by vapour transport [4,5], was cleaved in situ at a pressure in the lower 10^{-10} mbar region. The surface quality was checked by low energy electron diffraction (LEED). The XPD measurements are done in a modified Vacuum Generators ESCALAB Mk II X-ray photoelectron spectrometer equipped with a fixed hemispherical electron energy analyzer, and a three-channeltron detection system, operated with a base pressure in the lower 10^{-11} mbar region. The X-ray tube contains a MgKα ($h\nu$ = 1253.6 eV) and SiKα ($h\nu$ = 1740 eV) twin anode. The samples are fixed on a computer-controled two-axis goniometer capable of scanning the emission angle over the full hemisphere above the surface [6–11]. Data has been collected up to 78° polar angle.

Thanks to the chemical sensitivity of the photoemission technique, the core levels of a given type of atom can be selected. The chosen outgoing photoemitted electrons exhibit a strong anisotropic angular intensity distribution related to the local geometry around the selected atom. The analysis of the obtained diffraction patterns is simplified for electron kinetic energies higher than approximately 500 eV by the so-called "forward focusing" effect. This effect consists in a strong intensity enhancement along the emitter-scatterer direction and more generally along densely packed atomic planes (resulting in so-called Kikuchi bands) and rows of atoms (corresponding to low-index crystallographic directions) [12].

Note that experimental diffractograms are acquired by simultaneously collecting electrons at two different kinetic energies: one exactly at the maximum of the Ta $4f_{7/2}$ photoemission line (E_{kin} = 1229 eV) and one sligthly above (E_{kin} = 1234 eV) to monitor the background intensity variation. The subtraction of the two signals, taking into account the channeltron sensitivities, allows to get rid of the inelastic electron background.

To simulate the XPD experiment, the cluster model approach of the EDAC (Electron Diffraction in Atomic Clusters) code [13] is used here. This code, based on the muffin-tin potential approximation [14], evaluates the MSC expansion implemented using a fully convergent recursion method.

The calculations are performed for the $1T$ crystallographic structure (space group $P\bar{3}m1$ and lattice parameters are $a = b = 3.36$ Å, $c = 5.85$ Å), for the Ta $4f_{7/2}$ core level electrons (E_{kin} = 1229 eV when excited with MgKα). Three Ta emitters distributed down to 13 Å below the surface are chosen. The calculations were performed for a temperature T = 300 K and thermal vibrations are introduced by means of non-zero Debye temperatures θ_D. To obtain a quantitative value for the agreement between calculated and measured diffractograms, an R-factor analysis based on the multipole expansion of the angular intensity distribution, i.e., the expansion into spherical harmonics, has been used [16,17]. Moreover, anisotropies of local interference features have been calculated.

Results and discussion

The MSC simulated diffractogram of a hypothetical hexagonal Ta structure is presented in Figure 2a besides an in-plane cut of the crystal structure in Figure 2b. The stereographically projected diffractogram is plotted using a linear gray scale with high intensity in white (the outer circle corresponds to grazing emission, whereas the center represents the normal emission direction). Three different Ta emitters are chosen. They are located in the center of the Figure 2b, one at the surface and the two others just below, in the second and third unit cells. The 6-fold symmetry of the calculation is evident in Figure 2a. Each peak of the diffraction pattern corresponds to a "forward focusing" direction and is directly linked to a Ta-Ta direction.

The 6 most intense peaks, closest to normal emission, defining a center hexagon (plotted with a white line),

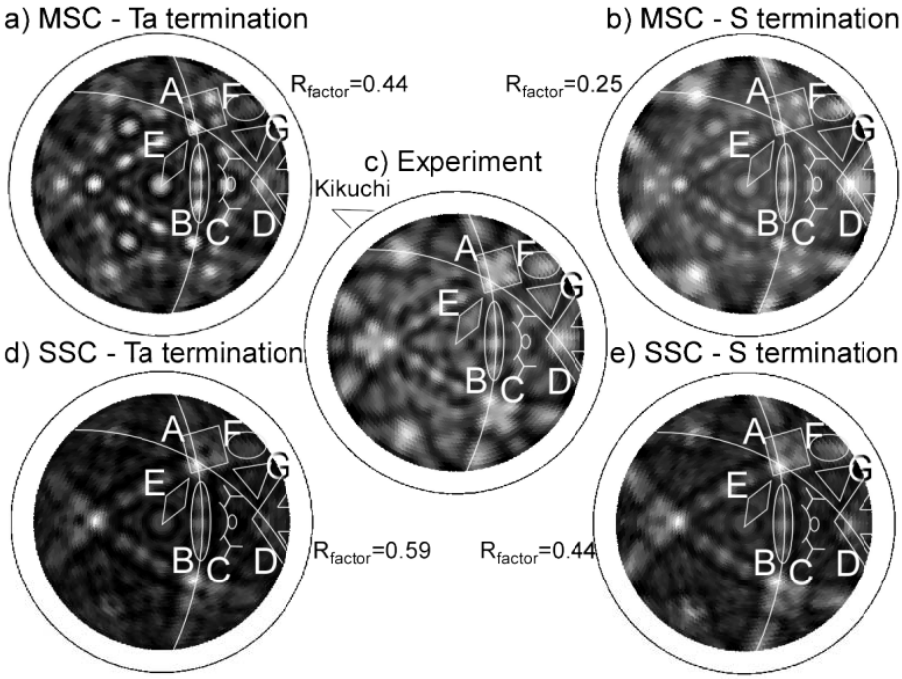

Fig. 3. Stereographic projections of (a) MSC calculated (Ta-termination), (b) MSC calculated (S-termination) , (c) measured, (d) SSC calculated (Ta-termination) and (e) SSC calculated (S-termination) diffractograms for Ta $4f_{7/2}$ emission at 1229 eV on a $1T$-TaS_2 (0001) surface.

are each surrounded by another hexagon (dashed line hexagon, displaced along the [1000] direction), and followed by another one (dotted). The hexagons are distorted in the diffractogram due to the stereographic projection. The discussed hexagons are plotted on the in-plane Ta structure in Figure 2b and illustrate how it is possible to attribute directly each "forward focusing" peak (Fig. 2a) to an emitter-scatterer direction.

The insertion of S atoms into the hexagonal Ta structure, as in the $1T$-TaS_2 structure, breaks the 6-fold symmetry of the clusters as shown in Figures 2c and 2d. MSC and SSC calculations are performed on both surfaces shown here. In the following, differences and similarities are discussed, first between the two terminations for the MSC and the SSC approaches separately and second between the two approaches.

Termination via multiple scattering

If the surface is either Ta-terminated (Fig. 3a), or S-terminated (Fig. 3b), the diffractograms become 3-fold symmetric, with the appearance of variations in the "forward focusing" peak intensities and the formation of other completely different structures.

In the theoretical and experimental data, see Figure 3, the "forward focusing" peaks are dominant, like in the hypothetical hexagonal Ta structure shown in Figure 2a. But, by introducing the S atoms, the 6-fold symmetry is broken. First, the feature labeled with A reveals four very sharp "forward focusing" peaks in the calculated Ta-terminated case, while there is more intensity inbetween in the experiment (Fig. 3c) and in the S-terminated case. This behavior is directly linked to the influence of the added uppermost S atom between the four Ta scatterers, see Figure 2d, which does not exist in the Ta-terminated structure. A similar behavior is visible in the B labeled region, along the Kikuchi bands, as well as in the C structure, where the "forward focusing" peaks are very sharp and clearly distinct in the Ta-terminated case while they appear connected in both the experiment and the S-terminated case simulation. Note that the B labeled region contains three peaks, but not with the same intensity. The middle peak is modulated by the two neighbouring "forward focusing" peaks aligned along the Kikuchi bands, see Figure 2d and by the presence or the absence of the S topmost layer. In the MSC S-terminated case and in the experiment (Figs. 3b and 3c), this middle peak has a higher intensity than the two outer ones neighbouring peaks, while it is the opposite for the Ta-terminated case (Fig. 3a).

The D labeled feature contains only a weak peak in the Ta-terminated case while it appears more intense and with a completely different shape in the S-terminated case, like in the experiment. The normal emission, which corresponds to the center of diffractograms, has a reduced intensity in the experiment and in the S-terminated MSC calculation, with respect to the Ta-terminated surface diffractogram. The opposite behavior is observed around the center, where the E labeled rhombus intensity is much weaker in the Ta-terminated case than in the two others diffractograms. Again, the formation of this centered three-branches star results from the scattering on the

S topmost layer, as shown in Figure 2d. The same observation can be made concerning the F (at the end of one Kikuchi band) and G regions.

So far, many similarities have been observed between the S-terminated crystal calculated case and the experiment and the agreement is better than for the Ta-terminated case. To evaluate the agreement between the complete experimental interference pattern data and the two theoretical cases, a global match approach, which uses the reliability R_{MP}-factor, is employed and confirms what has been observed locally. The much smaller value obtained for the S-terminated case, $R_{MP} \approx 0.25$, than for the Ta-terminated case, $R_{MP} \approx 0.44$, confirms what has been obtained by eye, which does not let any doubt on the S termination.

Termination via single scattering

As shown in Figures 3d and 3e, the S insertion into the hexagonal Ta structure also breaks the 6-fold symmetry, as in the MSC case. Globally, the same regions of the diffractograms can be detailed, but in the SSC case, the peaks are larger and some structures are missing in the diffraction patterns.

In the experiment (Fig. 3c), the A labeled region contains four peaks of almost equal intensity while there is a clear lack of intensity for the most external peak in the SSC calculations. For both terminations, this lack is filled using the MSC approach proving the necessity of working with MSC in this system to accurately simulate the diffraction patterns. The B region is broader using the SSC as compared to MSC and the modulation of the middle peak intensity (as discussed above) is not as visible in Figures 3a and 3b as in Figures 3d and 3e. Indeed the three peaks contained in the B region have almost the same intensity in the SSC for both terminations, contrary to the MSC case. The C, D and G labeled regions show almost no intensity in the SSC calculations as compared to the experiment. However, the E and F regions are well reproduced by the SSC.

As well as for the MSC approach, we use the reliability R_{MP}-factor to quantify the agreement between the complete experimental interference pattern data and the two theoretical cases. The smaller value obtained for the S-terminated case, $R_{MP} \approx 0.44$, than for the Ta-terminated case, $R_{MP} \approx 0.59$, indicates a better agreement for the S terminated surface. But the result is not as evident as for the MSC result since first, the feature shapes are broader and second, some structures are missing in SSC compared to the experiment, involving a weaker confidence in the SSC result. These differences result from known effects described in reference [1]. In fact, the scattering on the first few atoms has a tendency to focus the emission in the emitter-scatterer direction while on the subsequent atoms MSC tends to defocus the signal. It is a clear indication for the necessity to use MSC in order to get precise information on the intensity and shape of the "forward focusing" peaks. Note that the better agreement is not only due to the overemphasized "forward focusing" peaks obtained with the SSC approach but also due to the better agreement of the interference fine structures comparing the MSC and the experimental result.

Multiple scattering vs single scattering

For a more detailed comparison of the agreement between the experiment and the simulations, the local anisotropy, $A = \frac{I_{max}(\theta,\phi) - I_{min}(\theta,\phi)}{I_{max}(\theta,\phi)}$, is calculated for different features. The anisotropy does not give information about similarities in the shape of particular features in the three different cases (Ta-terminated surface, S-terminated surface and experiment) but indicates the intensity variations only.

The local anisotropy calculated for the different features are generally closer to the experiment for the S-terminated surface. For example, the anisotropies for the A labeled feature are 33.2% for the experiment, 44.8% and 46.7% for the MSC for the S- and Ta-termination while they are 69.3% and 76.2%, respectively, for the SSC approach. In this later case, the local anisotropies are much larger than those of the experiment. The same behavior is observed for the B, C, and D features.

Moreover, to obtain a quantitative indication of the diffraction pattern intensity variation owing to the S topmost layer, the two different diffractograms (S- and Ta-terminated surface) have been subtracted and then normalized as shown in equation (1). Note that both clusters have the same reference system to insure that the signal attenuation due to the escape depth is equal and thus that the calculated difference only contains information about the S topmost layer presence. $I_{Diff}(\theta,\phi)$ is given by:

$$I_{Diff}(\theta,\phi) = \frac{|I_{S-term}(\theta,\phi) - I_{Ta-term}(\theta,\phi)|}{(I_{S-term}(\theta,\phi) + I_{Ta-term}(\theta,\phi))/2} \quad (1)$$

and is plotted in Figures 4a and 4b for the SSC and MSC approaches. A larger difference is obtained for grazing emission angles, for both the SSC and MSC calculations. This is a logic consequence of the fact that by looking at grazing angle, the surface contribution is amplified compared to the one of the bulk. Indeed, the signal decreases proportionately to $e^{-\frac{d}{\lambda}}$, where λ is the electron inelastic mean free path and d is the path length. Emission from deeper lying emitters is thus strongly attenuated since it corresponds to long paths d at grazing emission.

Near normal emission, $I_{Diff}(\theta,\phi)$ is only significant in the MSC case. This variation corresponds to the bulk emission sketched in Figure 4. In SSC, the final emitted signal along a given "forward focusing" direction is proportional to the same emitter-scatterer signal multiplied by $e^{-\frac{d_1}{\lambda}} + e^{-\frac{d_2}{\lambda}} + ...$, where $d_i, i = 1, 2, ...$, are the emitter depths, depending on the number of emitters taken into account.

On the contrary, in MSC each scattering process (in all directions) contributes to modify independently the emitter-scatterer signal coming from the different emitters. It involves an intensity transfer (which is not considered in the SSC approach) between all the scatterers.

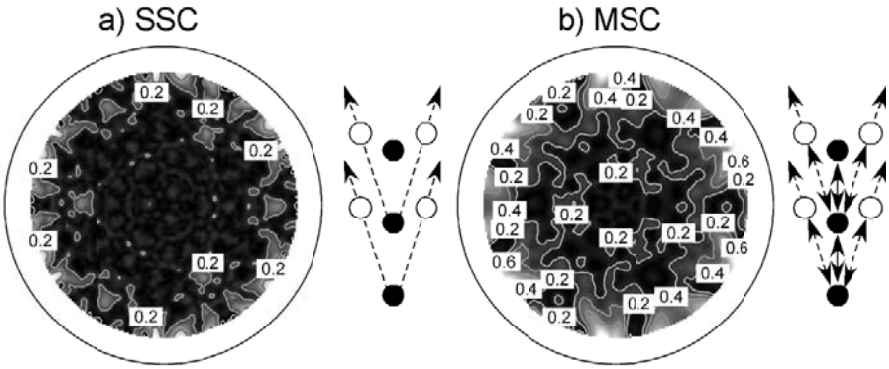

Fig. 4. $I_{Diff}(\theta, \phi)$ calculated for the (a) SSC and the (b) MSC approaches. The contour plots indicate the larger differences in both cases.

As all the emissions are finally scattered by the topmost layer before escaping, the scattering contribution of the surface atoms is increased, leading to an enhancement of the influence of the surface termination.

This result is corroborated by the difference in the R_{MP} which can also be interpreted in these terms. Indeed, the difference in the R_{MP} between both terminations is 0.19 for the MSC (reduction of 76%) while it is 0.15 for the SCC (reduction of 34.1%). It indicates that there are less differences between the two terminations relative to the experiment for the SSC approach compared to MSC, leading to a larger sensitivity of the MSC to the S termination.

Generalization

In this section, key points to determine the surface termination for bulk-emission with the MSC approach are discussed. Based on the above results, and to obtain a quantitative indication about the nature of the surface topmost layer, we compare $\langle I_{Diff}(\theta, \phi)\rangle$ averaged over all (θ, ϕ) angles for different cases, thereby giving a simple measure to differentiate the two surface terminations. Three different parameters are modified, the c-axis parameter, the scatterer type and the stacking sequence. The other parameters are fixed, leading to hypothetical materials systems.

$\langle I_{Diff}(\theta, \phi)\rangle$ is shown in Figure 5 for c-axis parameters between 5.853 (bulk value) and 3.75 Å, for different kinds of scatterers (O, S, Se), and for the two most natural stacking sequences, the so-called $1T$ and $2H$ polytypes. The values obtained for the case studied in Figure 4 ($c = 5.853$ Å, $1T$-TaS_2) are reported in Figure 5, left. First, as the c-axis becomes smaller, $\langle I_{Diff}(\theta, \phi)\rangle$ decreases. This is due to the increasing contribution of the bulk emission to the whole signal due to the electron inelastic mean free path. Indeed, as the c-axis is reduced, the emitter depths are also reduced and the signal coming from deep emitters is less attenuated. Consequently, the contribution of the topmost layer emission, and thus the difference between both terminations, is reduced relative to the whole signal. As plotted in Figure 5, this attenuation is weakly dependent on the scatterer type. Nevertheless the $\langle I_{Diff}(\theta, \phi)\rangle$ variation as a function of the c-axis value becomes larger for heavy scatterers.

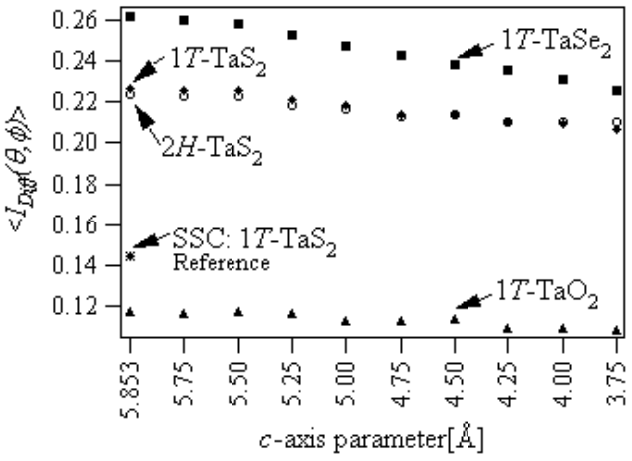

Fig. 5. $\langle I_{Diff}(\theta, \phi)\rangle$ calculated for different c-axis parameters, kind of scatterers and stacking sequences. The value obtained with the SSC approach shown in Figure 4 is reported here as reference. The filled and empty markers correspond to the $1T$ and $2H$ stacking sequences respectively.

Next, we substitute the S atoms of the $1T$-TaS_2 structure by two other scatterers, namely O and Se atoms. By changing scatterers, phase shifts are naturally changed, affecting the scattering strengths. This effect is well seen in Figure 5. When S atoms of the $1T$-TaS_2 are substituted by O atoms, $\langle I_{Diff}(\theta, \phi)\rangle$ drastically decreases, and becomes even lower than the reference value obtained by the SSC approach. For such a substitution, the Ta-Ta emission dominates the entire diffraction pattern and at the same time the Ta-O scattering becomes negligible [18]. This observation suggests that for too light scatterers (small scattering strength), it becomes very difficult to determine the surface termination for bulk-emission with this method. However, when S atoms of the $1T$-TaS_2 are substituted by Se atoms, $\langle I_{Diff}(\theta, \phi)\rangle$ increases, leading to a larger sensitivity to the surface topmost layer.

Finally, $\langle I_{Diff}(\theta, \phi)\rangle$ has been calculated for the $2H$-TaS_2 stacking sequence. As shown in Figure 5,

both $1T$ and $2H$ stacking sequences exhibit a similar $\langle I_{Diff}(\theta, \phi)\rangle$, indicating that the stacking is not crucial for the surface topmost layer determination procedure.

The best R_{MP} has been obtained for the $1T$ stacking sequence, the c-axis parameter corresponding to 5.95 Å (corresponding to a slight (2%) surface relaxation) and obviously using S atoms as scatterers. For comparison, $R_{MP} \approx 0.31$ and 0.55 have been obtained with the $2H$ stacking for the S- respectively Ta- surface termination. This R_{MP} is worse (by ≈28%) than what is obtained for the $1T$ polytype (0.25, 0.44) showing the sensitivity of XPD to the stacking sequence.

Conclusion

In all the presented experimental and calculated diffractograms, diffraction patterns are dominated by the "forward focusing" peaks along low-index crystallographic directions. But as seen, the variations of the peak widths, shapes and intensities are also strongly linked to the S atom presence at the surface. A larger confidence can be obtained with the MSC approach owing to a better agreement with the experiment (seen by eye and calculated via the R_{MP}-factor). Moreover, it appears that the contribution of the topmost S layer is quantitatively very strong in the MSC approach, which permits to clearly distinguish both terminations. It is shown that the full hemispherical XPD combined with the MSC approach is a powerful method to determine the surface termination for bulk-emission and may be applied to similar systems in the future.

A generalization of this approach for other systems is discussed. It appears that for a chosen emitter it becomes very difficult to determine the surface termination with this method for too light scatterers. Finally, by comparing the R_{MP} for the two most natural polytypes ($1T$, $2H$) it is shown that XPD is also sensitive to the stacking sequence.

We would like to thank the whole Neuchâtel workshop and electric engineering team for efficient technical support. This project has been supported by the Fonds National Suisse pour la Recherche Scientifique.

References

1. L. Despont, D. Naumović, F. Clerc, C. Koitzsch, M. Garnier, F.G. de Abajo, M.V. Hove, P. Aebi, Surf. Sci. **600**, 380 (2006)
2. B.J. Mrstik, R. Kaplan, T.L. Reinecke, M.V. Hove, S.Y. Tong, Phys. Rev. B **15**, 897 (1977)
3. M. Kasch, E. Pehlke, W. Schattke, T. Kurberg, H.P. Barnscheidt, R. Manzke, M. Skibowski, Surf. Sci. **214**, 436 (1989)
4. B. Dardel, M. Grioni, D. Malterre, P. Weibel, Y. Baer, F. Lévy, Phys. Rev. B **45**, 1462 (1992)
5. B. Dardel, M. Grioni, D. Malterre, P. Weibel, Y. Baer, F. Lévy, Phys. Rev. B **46**, 7407 (1992)
6. J. Osterwalder, T. Greber, A. Stuck, L. Schlapbach, Phys. Rev. B **44**, 13764 (1991)
7. D. Naumović, A. Stuck, T. Greber, J. Osterwalder, L. Schlapbach, Phys. Rev. B **47**, 7462 (1993)
8. R. Fasel, P. Aebi, J. Osterwalder, L. Schlapbach, Surf. Sci. **331–333**, 80 (1995)
9. J. Osterwalder, P. Aebi, R. Fasel, D. Naumović, P. Schwaller, T. Kreutz, L. Schlapbach, T. Abukawa, S. Kono, Surf. Sci. **331–333**, 1002 (1995)
10. D. Naumović, J. Osterwalder, A. Stuck, P. Aebi, L. Schlapbach, Surf. Sci. **287–288**, 950 (1993)
11. T. Greber, J. Osterwalder, D. Naumović, A. Stuck, S. Hüfner, L. Schlapbach, Phys. Rev. Lett. **69**, 1947 (1992)
12. C.S. Fadley, *Synchrotron Radiation Research: Advances in Surface Science* (Plenum, New York, 1990)
13. F.J. Garcia de Abajo, M.A. Van Hove, C.S. Fadley, Phys. Rev. B **63**, 075404 (2001)
14. J.B. Pendry, *Low Energy Electron Diffraction* (Acamedic Press, London, 1974)
15. J.J. Rehr, R.C. Albers, Phys. Rev. B **41**, 8139 (1990)
16. R. Fasel, P. Aebi, J. Osterwalder, L. Schlapbach, R.G. Agostino, G. Chiarello, Phys. Rev. B **50**, 14516 (1994)
17. R. Fasel, *Adsorbed monolayers and submonolayers studied by angle-scanned photoemission*, Ph.D. thesis, University of Fribourg (1996)
18. L. Despont, C. Lichtensteiger, F. Clerc, M.G. Garnier, F.G. Garcia de Abajo, M.V. Hove, J.-M. Triscone, P. Aebi, Eur. Phys. J. B **49**, 141 (2006)